Activation of the Insulin Receptor's Kinase Domain Changes the Rate-Determining Step of Substrate Phosphorylation†

Ararat J. Ablooglu and Ronald A. Kohanski*

Department of Biochemistry and Molecular Biology, Box 1020, The Mount Sinai School of Medicine, New York, New York 10029

Received September 29, 2000; Revised Manuscript Received November 13, 2000

ABSTRACT: The insulin receptor and many other protein kinases are activated by relief of intrasteric inhibition that is regulated by reversible phosphorylation. The changes accompanying activation of the insulin receptor's kinase domain were analyzed using steady-state kinetics, viscometric analysis, and equilibrium binding measurements. Peptide phosphorylation catalyzed by the unphosphorylated basal-state kinase is limited by a slow rate of the chemical step, and the activated enzyme is limited by product release rates. Underlying these changes were a 36-fold increase in the rate constant for the chemical step of the enzyme-catalyzed reaction, a 5-fold increase in the affinity for MgATP, and an 8-fold increase in the affinity for peptide substrate. This results in binding of substrates that is 2.2 kcal/mol more favorable and a free energy barrier for transition state formation that is lowered by 2.1 kcal/mol in the activated enzyme. Therefore, the change in conformational free energy inherent in the protein after autophosphorylation [Bishop, S. M., Ross, J. B. A., and Kohanski, R. A. (1999) *Biochemistry 38*, 3079−3089] is equally distributed between formation of the substrate ternary complex and formation of the transition state complex.

Most receptor tyrosine kinases are monomers in the absence of their ligands. Ligand binding to their extracellular domains induces dimerization, which in turn results in autoactivation through phosphorylation of multiple tyrosine residues in their intracellular kinase domains (*1*). These modifications create high affinity binding sites for their substrates and/or result in conformational changes leading to high activity states (*2*). In the case of the insulin receptor, however, the receptor is already a disulfide-linked dimer in the absence of insulin (*3*), and signaling events still require insulin binding (*4*). Therefore, it has been of a great interest to establish the differences in catalytic properties of the insulin receptor between its basal and activated states.

To study kinase activation, the insulin receptor's kinase domain (IRKD),[1,2] including all of the intracellular residues from R953 to S1355 (*5*, *6*), can be expressed as an enzymatically active recombinant protein using a baculovirus expression system. The IRKD in its unphosphorylated state mimics the native insulin receptor (IR) in its unphosphorylated basal state (*7*). Regulation by autophosphorylation is a feature of the native insulin receptor that is present both in the IRKD and the conserved catalytic core (*8*−*13*). Specifically, autophosphorylation of the IR or the IRKD "core" (see below) produces ≥200-fold increased catalytic efficiency (*10*−*13*). Autophosphorylation of tyrosines Y1162 and Y1163 in the activation loop (residues G1149 to P1172) are sufficient to produce this activation in all forms of the IR kinase (*12*−*16*). Use of a soluble recombinant protein at readily determined concentrations simplifies quantitative kinetic characterization of features that maintain the basal state and the changes that result from activation.

There are two structures of the conserved catalytic core of the IRKD, encompassing V978 to K1283 (*17*, *18*), which provide insight into the structural basis of the low activity basal state and the potential roles of autophosphorylation in the activated enzyme. The activation loop of the kinase domain is an intrasteric inhibitor in the basal state because it was found to occupy the active site cleft of the unphosphorylated protein (*17*); intrasteric inhibition regulates the catalytic activity of many protein kinases (*19*). Our previous in vitro solution studies revealed that the basal IRKD is in fact ≥90% in this intrasterically inhibitory conformation (*20*), and this *conformational* hindrance is relieved by activation loop phosphorylation (*17*−*21*). With the relief of intrasteric inhibition, there should be improved affinities for substrates. Along with the anticipated steric effects, there may be changes in the alignments of catalytically important residues that would have consequences for the chemical step of phosphoryl transfer (*17*, *18*, *22*, *23*). Here we have used steady-state kinetic analysis, equilibrium binding, and viscometric studies to identify stepwise differences and substrate affinity changes that distinguish basal-state from activated-state kinase domains of the insulin receptor.

† Supported by Grant DK50074 (R.A.K.) from the National Institutes of Health.

* To whom correspondence should be addressed. Phone: (212) 241-7288. Fax: (212) 996-7214. E-mail: Ronald.Kohanski@.mssm.edu.

[1] Abbreviations: Ac, acetate; AMP-PNP, adenosine 5′-(β,γ-imido)-triphosphate; PKA, cyclic-AMP dependent protein kinase; DTT, dithiothreitol; EDTA, ethylenediaminetetraacetic acid; IR, insulin receptor; IRKD, insulin receptor's kinase domain; pY, phosphotyrosine; Tris, tris(hydroxymethyl)-aminomethane.

[2] Numbering of the IR, IRKD and the conserved catalytic core is from Ebina et al. (*5*).

10.1021/bi002292m CCC: $20.00
Published on Web 12/19/2000

EXPERIMENTAL PROCEDURES

Materials. Dithiothreitol (Sigma Ultra), the disodium salt of ATP (from equine muscle, catalog no. A-5394), ADP, and bovine serum albumin (BSA, radioimmunoassay grade) were purchased from Sigma; hydrogenated Triton X-100 (protein grade) was from Calbiochem; EDTA was from Fluka; Tris acetate, base, and HCl, the ATP analogues adenosine 5′-(β,γ-imido)triphosphate (AMP-PNP, tetralithium salt), adenosine 5′-*O*-(3-thiotriphosphate) (ATPγS), and electrophoresis reagents were from Boehringer Mannheim; magnesium acetate ($MgAc_2$, enzyme grade) was from Fisher. Insect cell culture media and fetal bovine serum were from Gibco/BRL. Synthetic peptides were prepared as carboxy-terminal amides and differed only in the presence of a Tyr, Phe, or phospho-Tyr (pY) as the eighth residue that is shown in bold font: Y-IRS939, REETGSE**Y**MNMDLG; F-IRS939, REETGSE**F**MNMDLG; pY-IRS939, REETGSE**pY**MNMDLG. The amino acid sequence of the "parent" tyrosyl-peptides is based on a phosphorylation site, Y^{939}, in insulin receptor substrate-1 (*24*, *25*). Peptides were synthesized using Fmoc chemistry, HPLC-purified, and confirmed by amino acid analysis and automated Edman degradation. A different synthetic peptide was used as substrate for the product inhibition studies because it had different retention times than Y-IRS939 or pY-IRS939 and therefore could be quantified in our HPLC-based assay (*26*). This peptide was synthesized with a free carboxylic acid at the C-terminus, with the sequence KKKLPATGDYMNMSPVGD and is called IRS727, which was also used in the ternary complex structure solved by Dr. Steve Hubbard (*18*). This peptide with L-tetrafluorotyrosine in place of tyrosine, F_4-IRS727 (*27*), was used in control reactions for viscometric measurements. Both IRS727 peptides were generously provided by Dr. Philip Cole.

Adenine nucleotides and synthetic peptides were dissolved in 50 mM TrisAc, pH 7.0, the pH was readjusted to 7.0 with the addition of dilute acetic acid and/or NaOH, and the concentrations were adjusted to the desired values for stock solutions. These stocks were kept at −20 °C for frequent use or at −80 °C for prolonged storage. Integrity of the reagents was checked periodically by reverse-phase HPLC (peptides) or by thin-layer chromatography (nucleotides). The concentrations of adenine nucleotides and synthetic peptides were determined spectrophotometrically using the following extinction coefficients: ATP and ADP, $\epsilon = 15\,300\ M^{-1}\ cm^{-1}$ at 259 nm; AMP-PNP and ATPγS, $\epsilon = 15\,000\ M^{-1}\ cm^{-1}$ at 260 nm; Y-IRS939 $\epsilon = 1300\ M^{-1}\ cm^{-1}$ at 278 nm; pY-IRS939, $\epsilon = 340\ M^{-1}\ cm^{-1}$ at 278 nm; F-IRS939, $\epsilon = 352\ M^{-1}\ cm^{-1}$ at 257 nm.

Protein Expression and Purification. Baculovirus encoding amino acid residues 953−1355 of the insulin receptor's cytoplasmic kinase domain was a generous gift of the late Dr. Ora Rosen (*6*). The mutant JMY2F-IRKD and the double truncation mutant ΔΔ-IRKD (residues 978−1283) mutant were subcloned in this laboratory (*20*) using a human insulin receptor cDNA kindly provided by Dr. Jonathan Whittaker (*28*). Wild-type and mutant kinase domains were expressed in "High Five" cells (Invitrogen), maintained at 27.5 ± 0.5 °C. The monolayers were grown to 60% confluence at the time of infection. Viral infection was done for 3−4 h at a multiplicity of infection of 9−10. The infection media was then replaced with fresh media. Cells were harvested at 53 h from the start of infection. Cells were resuspended in homogenization buffer (250 mM sucrose, 50 mM Tris base, 20 mM NaCl at pH 7.5) and stored at −80 °C, at least overnight. IRKD purification was done as described in Bishop et al. (*21*). The purified protein was quantified spectrophotometrically at 278 nm ($\epsilon = 40\,200\ M^{-1}\ cm^{-1}$) and stored at −20 °C in 38% glycerol (w/w). The double truncation mutant ΔΔ-IRKD, both unphosphorylated and after autophosphorylation, was used for the equilibrium binding and viscometric measurements. Its basal-state and activated-state kinetic properties were the same as those of the unphosphorylated JMY2F-IRKD and autophosphorylated full-length wild-type IRKD, respectively (not shown). Furthermore, our previous reports demonstrated that core flanking regions do not have any statistically significant effect on the kinase activation process or maximum specific activity (*20*). Using the double truncation mutant ΔΔ-IRKD for the basal state avoids partial activation coincident with juxtamembrane autophosphorylation (a phenomenon described previously, ref *29*). It is also easier to generate and re-isolate the activated state of the double truncation mutant ΔΔ-IRKD in higher yields because there are only three autophosphorylation sites, as described by Wei et al. (*13*).

Autophosphorylation of the Kinase Domain. Wild-type IRKD (or double truncation mutant ΔΔ-IRKD) was autophosphorylated according to Ablooglu et al. (*27*). The reaction was for 60 min at 5 mM ATP, 20 mM $MgAc_2$ in 50 mM TrisAc, 5 mM DTT, and 0.05% hydrogenated Triton-X 100, pH 7.0, at room temperature. Autophosphorylated kinase was repurified by anion exchange chromatography after initial removal of small reactants and products using electro-elution. Preliminary experiments established conditions for IRKD and ATP concentration and time of autophosphorylation that produced the highest specific activity. The maximally activated kinase domain was characterized by its increased mobility in nondenaturing PAGE as described previously (*30*), specific activity, and peptide mapping: Autophosphorylation of tyrosines in the activation loop was determined by reverse-phase HPLC mapping of peptides from an endoproteinase Lys-C digest; the activation loop was ∼80% trisphosphorylated plus ∼20% bisphosphorylated, and there was no evidence for unphosphorylated or monophosphorylated activation loop peptides (not shown). The activated kinase was stored in 38% glycerol (w/w) at −20 °C. The concentration of phospho-IRKD was determined spectrophotometrically, using an extinction coefficient $\epsilon = 35\,200\ M^{-1}\ cm^{-1}$ at 278 nm at pH 7.0 in 50 mM TrisAc. The lower extinction coefficient was due to the lower molar absorption by *phospho*tyrosine as compared to tyrosine.

Steady-State Kinetics. Steady-state kinetic parameters were determined using an HPLC-based assay (*26*, *27*). Reactions were performed at room temperature in 50 mM TrisAc, 5 mM DTT, 0.05% BSA (w/v), 2−8 nM phospho-IRKD, 20 mM $MgAc_2$, 40−160 μM IRS939, and 40−160 μM ATP. Dead-end inhibition studies were done using F-IRS939 over the range 180−800 μM, or AMP-PNP over the range 200−800 μM. The constant substrate concentrations were 40 μM ATP with variable Y-IRS939, or 80 μM Y-IRS939 and variable ATP concentration. Product inhibition studies were done with ADP over the range 50−200 μM, with 60 μM

ATP and variable Y-IRS939 or 60 μM Y-IRS939 and variable ATP. Product inhibition by pY-IRS939 was over the range 600−1500 μM at fixed 80 μM ATP and variable IRS727, or 150 μM IRS727 and variable ATP; $K_{M,\ IRS727}$ = 180 ± 20 μM at pH 7.0 (*27*). The reactions with variable peptide concentrations were initiated with the addition of ATP, and those with variable ATP were initiated by the addition of peptide. Reactions using the JMY2F mutant as the basal state enzyme were done as described previously (*30*). To determine K_i for both dead-end inhibitors in the basal state, using JMY2F, the concentrations of AMP-PNP were varied between 1 and 4 mM at constant 0.5 mM Y-IRS939 and variable ATP from 0.5 to 5.0 mM. The concentrations of F-IRS939 were varied between 0.5 and 4 mM at constant 2 mM ATP and variable Y-IRS939 from 0.5 to 2.5 mM. Inhibition constants were determined from the best global fit for linear competitive inhibition.

Steady-state kinetic parameters of the maximally autophosphorylated kinase were fit to the random-order rapid-equilibrium Bi Bi reaction mechanism (*31*−*33*), which is also the mechanism suggested for the partially purified full-length IR (*34*). Global fitting of the data was done using SigmaPlot and the following equations. For a sequential two-substrate kinetic mechanism,

$$v_i = \frac{V_{max}AB}{K_{ia}K_b + K_aB + K_bA + AB} \quad (1)$$

where the substrate concentrations are indicated by *A* and *B*, the K_M for each substrate is indicated by K_a and K_b, and K_{ia} is the binding constant for substrate *A*. For data with variable dead-end or product inhibitors that are competitive or noncompetitive against variable substrate *S* (i.e., variable substrate *A* with fixed substrate *B*) the following equations were used:

$$v_i = \frac{V_{max}S}{K_M(1 + I/K_i) + S} \quad (2)$$

$$v_i = \frac{V_{max}S}{K_M(1 + I/K_i) + S(1 + I/K_i)} \quad (3)$$

where *I* is the inhibitor concentration and K_i is the dissociation constant for the inhibitor (*31*).

Equilibrium Binding Measurements. There is a nucleotide-dependent decrease in the intrinsic fluorescence of the basal-state kinase when measured in the presence of potassium iodide. Steady-state fluorescence emission spectra were obtained with an SLM 4800 spectrofluorometer operating in the single-photon counting mode. The excitation polarizer was set at 55° and the emission polarizer was set at 0° to avoid the Wood's anomaly of the emission grating. An excitation wavelength λ_{ex} = 300 nm was used to reduce primary absorbance effects (inner filter errors) from high concentrations of nucleotides. The excitation slit and emission slits were set at 8 nm band-pass. Integrated fluorescence intensity was taken from emission spectra collected over the range 310 nm ≤ λ_{em} ≤ 420 nm with 1-nm increments, and the final spectra were determined from the average of three data points at each wavelength. All fluorescence experiments were done at 21 °C.

The conditions for nucleotide binding measurements were 1 μM IRKD, 0.4 M KI, 0.2 M KCl, 1 mM $Na_2S_2O_3$, 50 mM TrisAc, 20 mM $MgAc_2$, 1 mM DTT, 0.05% hydrogenated Triton X-100 (v/v), pH 7.0. Sixty-three microliters of the kinase mixture was mixed with 7 μL of 10-fold concentrated nucleotide to a final volume of 70 μL. Sixty microliters of this kinase/nucleotide mixture was used to obtain fluorescence emission spectra. The fluorescence quenching data were first corrected with the blank spectrum taken without IRKD. An additional correction for primary absorbance effects was made as described in Birsdall et al. (*35*). The absorbance filtering effects at high concentrations of adenine nucleotide, which occurred even with λ_{ex} = 300 nm, were determined by loss of fluorescence from a stock 2 μM *N*-acetyltryptophan amide (NATA) solution, where binding between NATA and adenine nucleotide does not occur over the concentrations of nucleotide employed. The decrease in the integrated fluorescence intensity was fit to a single exponential

$$FI_{obs} = FI_0 e^{-bL} \quad (4)$$

where FI_{obs} is the integrated fluorescence intensity (FI) at the concentration of adenine nucleotide (ligand for the IRKD; *L*), FI_0 is the FI observed in the absence of any ligand, and *b* is the emperically determined postexponential coefficient that describes dependence of the inner filter effect on ligand concentration. For ADP, $b = 0.021 \pm 0.002$ mM^{-1} (n = 14; $r = 0.945$; $p < 0.0001$).

Binding data were analyzed by nonlinear least-squares fitting to a hyperbolic (saturable) decrease in FI_{obs} to variable *L*,

$$FI_{obs} = FI_0 - \Delta FL/(K_d + L) \quad (5)$$

where ΔF is the maximum decrease in FI extrapolated to saturating ligand concentrations, and K_d is the dissociation constant. Because the total ligand concentration was in large excess over kinase concentration, *L* was taken as the free ligand concentration in these equations. Binding data are displayed as fractional saturation versus ligand concentration.

Viscometric Measurements. The viscosity dependence for k_{cat} and k_{cat}/K_M were determined using sucrose as the microviscogen and poly(ethylene glycol) (PEG 8000) as the macroviscogen in control reactions, following published procedures (*36*, *37*). Phosphoryl transferase reactions with phosphorothioates (e.g., ATPγS) tend to be slower than the corresponding phosphoryl transfers and are chemistry-limited (*38*−*40*). Similarly, we have reported characteristics for a peptide substrate of the activated kinase with poor turnover but a fairly average Michaelis constant (*27*); the tetrafluorotyrosyl peptide F_4-IRS727 ($k_{cat} = 0.5 \pm 0.1$ s^{-1}, K_M = 0.21 ± 0.05 mM). Therefore, ATPγS and F_4-IRS727 were used as controls for nonspecific effects of viscogens on the measurements of k_{cat}. The solution viscosities were determined using an Ostwald capillary viscometer maintained at 24 ± 0.1 °C in a temperature-controlled circulating water bath, and the relative viscosity (η^{rel}) was calculated with the following equation:

$$\eta^{rel} = \frac{t^0}{t} \cdot \frac{\rho}{\rho^0} \quad (6)$$

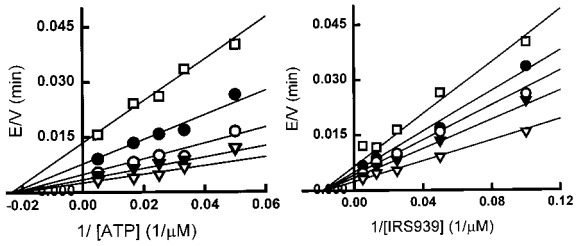

FIGURE 1: Steady-state kinetics of peptide substrate phosphorylation by the activated IRKD. Double reciprocal plots from measurements of initial velocity versus ATP concentration (left) and peptide substrate concentration (Y-IRS939; right). Initial velocities are expressed as mol of phosphopeptide formed (mol of kinase)$^{-1}$ min^{-1}. The following substrate concentrations (μM) were used: ATP, 20 (□), 40 (●), 60 (○), 100 (▼), and 200 (△); Y-IRS939, 10 (□), 20 (●), 40 (○), 60 (▼), and 200 (△). Reaction conditions are given under Experimental Procedures.

where t^0 and t are the transit times for a given standard and viscous buffer, respectively, and ρ^0 and ρ are the densities of the standard and viscous buffers, respectively (*41*). The standard buffer was 50 mM TrisAc, pH 7.0. Viscosity dependencies of k_{cat} were done as follows: 0.2 μM basal-state kinase, 0.13−2.66 mM Y-IRS939, constant 8 mM ATP, and then extrapolated to saturating substrate by fitting the observed k_{cat} versus peptide concentration to a rectangular hyperbola. Reactions with 3 nM activated kinase were done at 1 mM ATP and 0.36 mM IRS939. To determine the viscosity dependencies for $k_{cat}/K_{M,ATP}$ measurements were done at 0.3 mM ATP and 2.7 mM IRS939 for the basal-state kinase, and at 0.015 mM ATP and 0.18 mM IRS939 for the activated kinase. To determine the viscosity dependencies for $k_{cat}/K_{M,Y-IRS939}$ measurements were done at 8 mM ATP, 0.36 mM Y-IRS939 for the basal-state kinase, and at 1 mM ATP, 0.027 mM IRS939 for the activated kinase. Reactions were done twice in triplicates. The results will be used to estimate a limited number of stepwise rate constants, as applied to protein kinases by Adams and Taylor (*42*) and in further detail by Wang et al. (*36*).

RESULTS

Steady-State Kinetic Parameters for the Activated Kinase. Primary initial velocity data were collected from five ATP concentrations and six Y-IRS939 concentrations. These were analyzed by global fitting using eq 1, and the results are shown in the double-reciprocal plots of Figure 1. The pattern of intersecting lines is consistent with a sequential addition of substrates. This analysis produced $k_{cat} = 8.3$ s^{-1}, $K_{M,MgATP} = 0.04$ mM, and $K_{M,Y-IRS939} = 0.05$ mM (Table 1). To better define the steady-state kinetic mechanism, substrate analogues were used as dead-end inhibitors; AMP-PNP was a competitive inhibitor against ATP and noncompetitive against Y-IRS939, and F-IRS939 was competitive against Y-IRS939 and noncompetitive against ATP. These findings with dead-end inhibitors are consistent with a rapid-equilibrium random-order mechanism. The inhibition constants K_i for each inhibitor, listed in Table 1, show that nucleotide binding is tighter than peptide binding. The product-inhibition patterns were also determined, showing that each product was a competitive inhibitor against both substrates, which supports a rapid-equilibrium random-order mechanism for the IRKD activated by autophosphorylation. This conclusion was reached previously for the autophosphorylated IR (*34*). The inhibition constants, listed in Table 1, also show that nucleotide binding is tighter than peptide binding. Inhibition by AMP was analyzed to determine its affinity for the activated kinase ($K_i = 0.31$ mM), which was similar to AMP-PNP ($K_i = 0.24$ mM). Finally, the reaction with ATPγS was analyzed for subsequent use in viscometric studies (below); the reaction showed $k_{cat} = 0.014$ s^{-1}, a 600-fold lower turnover number than for ATP. Because of this low rate, binding of this nucleotide to the kinase was readily analyzed by inhibition of the ATP-dependent peptide phosphorylation reaction, yielding $K_i = 0.21$ mM ATPγS (Table 1).

Table 1: Kinetic Parameters for Substrates and Inhibitors of the Insulin Receptor Kinase Domain in the Activated and Basal States

	IRKD[a]	
parameter	activated	basal
k_{cat} (s^{-1})	8.3 ± 0.7	1.2 ± 0.3
	Nucleotides (mM)	
$K_{M\ ATP}$	0.04 ± 0.01	1.0 ± 0.3
$K_{i\ AMP-PNP}$	0.24 ± 0.04	>2[b]
$K_{i\ ADP}$	0.03 ± 0.01	1.1 ± 0.2[b]
$K_{i\ AMP}$	0.31 ± 0.04	>10[b]
$K_{i\ ATP\gamma S}$	0.21 ± 0.04	nd
	Peptides (mM)	
$K_{M\ Y-IRS939}$	0.05 ± 0.01	∼2
$K_{i\ F-IRS939}$	1.1 ± 0.1	∼2
$K_{i\ pY-IRS939}$	1.7 ± 0.9	3.1 ± 0.3

[a] The activated IRKD is the maximally autophosphorylated protein and basal IRKD is the unphosphorylated protein. [b] Values of the dissociation constants K_d were also determined from equilibrium binding measurements (Figure 2): 3.2 ± 0.6 mM AMP-PNP, 1.1 ± 0.2 mM ADP, and >100 mM AMP.

Steady-State Kinetic Parameters for the Unphosphorylated Kinase. We have reported previously some of the basal-state kinetic parameters (*29*). We have repeated the data obtained originally with the JMY2F mutant, now using the double-truncation mutant, and report the best estimates for $k_{cat} = 1.2$ s^{-1} and K_M values in the millimolar range for both substrates (Table 1). In addition, we have expanded the data to include inhibition constants for nucleotides and peptides for comparison with the activated enzyme (Table 1). These results show that nucleotide binding affinities change dramatically and that AMP has extraordinarily weak binding to the basal-state enzyme, since it fails to inhibit the kinase reaction at concentrations as high as 10 mM. However, the low turnover number and millimolar K_M and K_i values required high concentrations of substrates and inhibitors for these analyses. Because those conditions produced poor signal-to-noise ratios in our HPLC-based assay (*26*), we could not obtain data of sufficient quality to analyze patterns in double-reciprocal plots nor to discriminate among formal mechanisms by curve fitting, and thus a formal steady-state kinetic mechanism could not be assigned with confidence to the basal-state kinase. These concerns about precision led us to develop an indirect assay for nucleotide binding at equilibrium to confirm the data from inhibition studies.

Equilibrium Binding of Adenine Nucleotides to the Unphosphorylated Kinase. Iodide quenching in the basal-state IRKD is minimal[3] (Figure 2, panel A, inset). In the presence

[3] Previous mutagenesis and iodide quenching studies showed that W1175, in the active site cleft, is the dominant fluorophore of the IRKD emission spectrum (*21*).

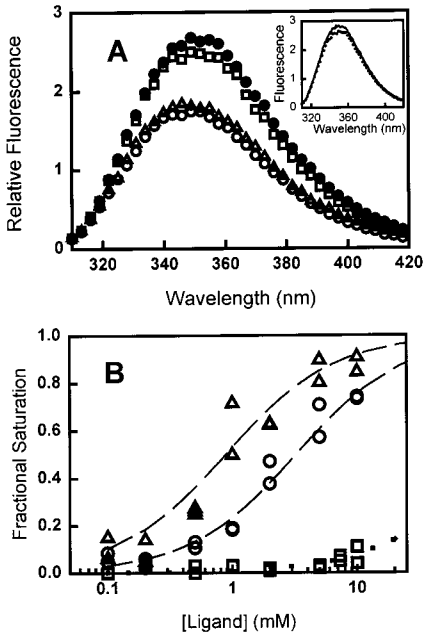

FIGURE 2: Nucleotide binding affinities to the basal-state kinase. Adenine nucleotide binding was determined by changes in iodide quenching of tryptophan fluorescence. Panel A: fluorescence emission spectra of 1 μM unphosphorylated (basal-state) IRKD in the presence of 0.4 M KI as quencher, taken in 50 mM TrisAc, pH 7.0, 0.2 M KCl, 1 mM DTT, 1 mM $Na_2S_2O_3$, and 20 mM $MgAc_2$,- with an excitation wavelength of 300 nm. Spectra for the kinase alone (●) and in the presence of 10 mM nucleotide analogues: AMP-PNP (○), ADP (△), AMP (□). Spectra have been corrected for blanks and inner filter errors arising from the high nucleotide concentrations, as described under Experimental Procedures (eq 4). The *inset* shows the fluorescence emission spectra of the unphosphorylated kinase at constant 0.6 M potassium salts: Solid line, 0.6 M KCl; dotted line, 0.4 M KI + 0.2 M KCl. Panel B: Binding data from iodide quenching at the indicated concentrations of adenine nucleotides are presented as fractional saturation for AMP-PNP (○), ADP (△), and AMP (□); data for AMP were analyzed assuming the same assay endpoint would be reached here as for AMP-PNP and ADP. The dashed lines were generated by nonlinear curve fitting to eq 5.

of 10 mM ADP or 10 mM AMP-PNP, there is significant quenching, but there is virtually no increase in iodide quenching induced by AMP at concentrations up to 10 mM (Figure 2, panel A). The increase in iodide quenching is dependent on the concentration of adenine nucleotide for AMP-PNP and ADP (Figure 2, panel B). Fitting these results for a single nucleotide binding site, we determined dissociation constants of 3.2 mM AMP-PNP, 1.1 mM ADP, and estimated K_d > 100 mM AMP from the marginal effect of this nucleotide on iodide quenching. These observations confirm the weak binding of nucleotides to the basal-state IRKD and support the findings from steady-state kinetics using both the JMY2F and double-truncation mutants of the kinase (Table 1).

Viscometric Changes in Steady-State Kinetic Parameters. Substrate binding and product release are diffusional steps in an enzyme catalyzed reaction that will be sensitive to changes in solution viscosity. In contrast, the chemical step-(s) should be insensitive to solution viscosity because these occur within the active site cleft, sequestered from exchange with the free ligands. These factors have been exploited widely to better understand the rate-limiting steps of enzyme catalysis (*38*, *42*−*47*). Here we used viscosity effects to determine whether rate constants for catalytic steps entailed

Scheme 1

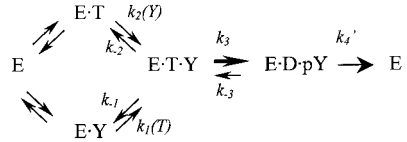

by k_{cat} and k_{cat}/K_M are subject to the same limitations before and after kinase activation.

A rapid-equilibrium random-order pathway accounting for steady-state kinetics of the activated IRKD is shown in Scheme 1 as a framework to interpret the viscosity-dependence experiments. The constants for addition of substrates MgATP (T) and tyrosyl-peptide (Y) are shown for the experimental conditions used to determine k_{cat}/K_M by saturating with one substrate and using low concentrations of the other substrate. Steps for release of products MgADP (D) and phosphotyrosyl-peptide (pY) are included in the net rate constant, $k_{4'}$. The equilibrium constant $K_{tc} = (E{\cdot}D{\cdot}pY)/(E{\cdot}T{\cdot}Y) = k_3/k_{-3}$ describes interconversion of the substrate and product ternary complexes; it probably favors the latter such that $k_3 > k_{-3}$ (see Discussion). For this mechanism and this assumption k_{cat} is defined by

$$k_{cat} = \frac{k_3 k_{4'}}{k_3 + k_{-3} + k_{4'}} \approx \frac{k_3 k_{4'}}{k_3 + k_{4'}} \qquad (7)$$

Increased viscosity will not change the chemical step's rate constant but will alter the diffusive step's rate constant $k_{4'}$ by a factor υ, where υ is proportional to $1/\eta^{rel}$. The ratio $\{k_{cat}\}^0$ in the absence of viscogen versus $\{k_{cat}\}^{\upsilon}$ in the presence of viscogen is

$$\{k_{cat}\}^{rel} = \frac{\{k_{cat}\}^0}{\{k_{cat}\}^{\upsilon}} = \frac{k_3 + \upsilon k_{4'}}{\upsilon(k_3 + k_{4'})} \qquad (8)$$

When $\{k_{cat}\}^{rel}$ is plotted versus η^{rel} the resulting line passes through the point (1,1) with a slope given by

$$\{k_{cat}\}^{\eta} = \frac{\{k_{cat}\}^{rel} - 1}{\eta^{rel} - 1} = \frac{k_3}{k_3 + k_{4'}} \qquad (9)$$

These equations will be used to calculate stepwise rate constants from the steady-state kinetic data and $\{k_{cat}\}^{\eta}$.

Control reactions for the effects of microviscogens on determination of kinetic parameters were performed first, using the activated IRKD. As shown in Figure 3, panel A, the macroviscogen PEG had a only slight effect on $\{k_{cat}\}^{rel}$, yielding a slope of -0.10 ± 0.10. This result suggested that subsequent effects of the microviscogen sucrose would be due to collisional effects on microsolutes. Reactions using sucrose with ATPγS showed no variation in $\{k_{cat}\}^{rel}$ with increasing viscosity. Similarly, k_{cat} measured with F_4-IRS727 showed no viscosity-dependent change. These results, expected for a chemical step-limited reaction (see Discussion) suggest there are no "chemical" effects of sucrose on either substrate (Y-IRS939 or MgATP, respectively) that would confound interpretation of the results, e.g., changes in the oxidation state or hydration state of the substrates (*37*, *47*).

Increasing viscosity changed k_{cat} for the activated kinase but not for the basal-state kinase (Figure 3, panel B). The positive slope for the activated kinase was 0.82 ± 0.08 which

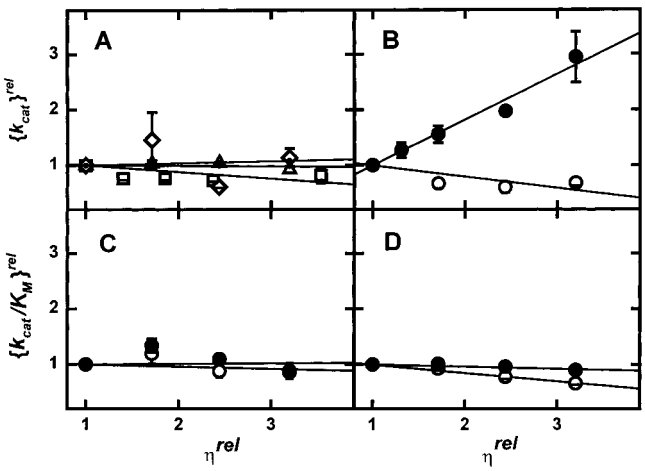

FIGURE 3: Viscosity dependence of steady-state kinetic parameters for the basal and the activated kinases. Plots of $\{k_{cat}\}^{rel}$ and $\{k_{cat}/K_M\}^{rel}$ versus relative viscosity η^{rel} are shown. Panel A: control experiments for $\{k_{cat}\}^{rel}$ using the activated IRKD. Viscosity was increased with the macroviscogen PEG8000 (□). Reactions using the microviscogen sucrose with ATPγS (△) and with F_4-Irs727 (◇). Panel B: plots of $\{k_{cat}\}^{rel}$ for basal kinase (●) and activated kinase (○). Panel C: plots of $\{k_{cat}/K_{M,MgATP}\}^{rel}$ for basal kinase (●) and activated kinase (○). Panel D: plots of $\{k_{cat}/K_{M,Y-IRS939}\}^{rel}$ for basal kinase (●) and activated kinase (○). Determinations were made in twice in triplicate. Data were fit by linear regression (solid lines).

Table 2: Kinetic Parameters Determined from Viscometric Experiments

parameter	activated IRKD	basal IRKD
	Observed	
$\{k_{cat}\}^{\eta}$	0.8 ± 0.1	0
$\{k_{cat}/K_{M,T}\}^{\eta}$	0	0
$\{k_{cat}/K_{M,Y}\}^{\eta}$	0	0
	Calculated[a,b]	
k_3 (s^{-1})	42 ± 26	1.2 ± 0.2
$k_{4'}$ (s^{-1})	10.5 ± 1.4	≥ 12
$K_{d,T}$ (mM)	0.25	1
$K_{d,Y}$ (mM)	0.20	2

[a] These parameters were calculated from the following relationships: In the activated state, $k_{4'} = k_{cat}/\{k_{cat}\}^{\eta}$; $k_3 = k_{cat}k_{4'}/(k_{4'} - k_{cat})$; $K_{d,Y} = K_{M,Y}(k_3 + k_{4'})/k_{4'}$ which is derived from the relationship $K_{M,Y} = k_{4'}(k_{-2} + k_3)/k_2(k_3 + k_{4'})$ at saturating nucleotide substrate *T* and the condition where $k_{-2} > k_3$ is satisfied under a rapid equilibrium mechanism (discussed in relation to Figure 1 and Table 1); $K_{d,T} = K_{M,T}(k_3 + k_{4'})/k_{4'}$ which is derived from the relationship $K_{M,T} = k_{4'}(k_{-1} + k_3)/k_1(k_3 + k_{4'})$ at saturating peptide substrate *Y* and the condition where $k_{-1} > k_3$ is satisfied under a rapid equilibrium mechanism. In the basal state, $k_3 \approx k_{cat}$ when $\{k_{cat}\}^{\eta} = 0$ because $k_{4'} \gg k_3$, thus setting a lower limit of $k_{4'} \geq 10k_3$; $K_{d,T}$ was determined by equilibrium binding (Figure 3); $K_{d,Y} \approx K_{M,Y}$ when $\{k_{cat}/K_{M,Y}\}^{\eta} = 0$ such that $k_{-2} \gg k_3$ and the condition $k_{4'} \gg k_3$ is also met (above). [b] Values are mean ± one standard deviation, calculated using the ranges for k_{cat} and $\{k_{cat}\}^{\eta}$.

indicates a partially diffusion-step limited reaction. The rate constants for the chemical and product release steps were calculated and indicate $k_3 \approx 4k_{4'}$ (Table 2). The absence of viscogen sensitivity shown by the basal-state kinase indicates this reaction is limited by the rate of the chemical step, such that $k_3 = k_{cat}$. Thus, $k_{4'} = 10k_3$, as indicated in Table 2. These constants were calculated as described in the footnote to Table 2.

To grasp the significance of the viscogen (in)dependence of k_{cat}/K_M this parameter is illustrated here for peptide at saturating MgATP,

$$k_{cat}/K_{M,Y} = \frac{k_2k_3k_{4'}}{k_{-2}k_{-3} + k_{-2}k_{4'} + k_3k_{4'}} \approx \frac{k_2k_3}{k_{-2} + k_3} \qquad (10)$$

where the assumption that $k_{4'} > k_{-3}$ (product release is faster than back-conversion of the product ternary complex) allows the last ratio to be used. Added viscogen will alter each diffusive step, k_2 and k_{-2}, by a factor υ and the relative change in k_{cat}/K_M is

$$\{k_{cat}/K_{M,Y}\}^{rel} = \frac{\{k_{cat}/K_{M,Y}\}^{0}}{\{k_{cat}/K_{M,Y}\}^{\upsilon}} = \frac{\upsilon k_{-2} + k_3}{\upsilon(k_{-2} + k_3)} \qquad (11)$$

Graphically, a plot of $\{k_{cat}/K_M\}^{rel}$ versus η^{rel} will pass through the point (1,1) and have a slope given by

$$\{k_{cat}/K_M\}^{\eta} = \frac{\{k_{cat}/K_M\}^{rel} - 1}{\eta^{rel} - 1} = \frac{k_3}{k_{-2} + k_3} \qquad (12)$$

For the nucleotide substrate MgATP (*T*), the viscosity dependencies follow the same rationale and equations for peptide substrate (*Y*), substituting k_1 and k_{-1} for k_2 and k_{-2}, respectively.

The parameter k_{cat}/K_M did not change with increasing viscosity for the basal-state or activated kinases for either substrate: the slopes given by $\{k_{cat}/K_M\}\eta$ were slightly negative at −0.01 and −0.04, for $k_{cat}/K_{M,ATP}$ in the basal-state and activated kinase, respectively (Figure 3, panel C), and slopes of −0.04 and −0.15 for k_{cat}/K_M in the basal-state and activated kinase, respectively (Figure 3, panel D). Because these slopes do not fall outside the range determined from control experiments, they are presented as zero-values in Table 2. For the activated kinase, this indicates the substrate ternary complex (E·T·Y) equilibrates rapidly with substrates versus its conversion to products, such that $k_{-2} \gg k_3$. In turn, this leads to dissociation constants for each substrate that are 5-fold greater than the corresponding Michaelis constants, which may be expected for a rapid-equilibrium random-order mechanism in which product release is partially rate-limiting (cf. ref *42*). For the basal state kinase, $k_{-2} \gg k_3$ from $\{k_{cat}/K_M\}\eta = 0$, and $k_3 \ll k_{4'}$ from $\{k_{cat}\}^{\eta} = 0$, together make K_M and K_d numerically equivalent (see footnote in Table 2). These values for substrate K_d's in the basal-state are listed in Table 2.

DISCUSSION

Differences in Steady-State Kinetic Parameters. We have clearly demonstrated that increased catalytic efficiency of the autophosphorylated kinase domain of the insulin receptor resulted from changes in k_{cat} and K_M for both substrates. Previous reports suggested that autophosphorylation of the insulin receptor caused a change in V_{max} (k_{cat}) without affecting K_M for the peptide substrates (*48*, *49*) and for ATP (*10*). These apparent discrepancies may have resulted from subtle details of the assay conditions. For example, use of protamine to activate the kinase or a Mn^{2+}/ Mg^{2+} mixture as the divalent metals for ATP may have been factors; the activation by polycations is complex and not fully reversible upon dilution (*10*, *50*), and choice of divalent metal ion has a significant impact on K_M for ATP (*29*, *40*). In addition, use of a peptide substrate with an intrinsically high K_M or in

which the reaction is limited by the chemistry (e.g., F_4-IRS727) could have masked changes in K_M.

It was hoped that changes in substrate binding affinities would be useful in quantitatively assessing relief of intrasteric inhibition. However, as shown by the K_i values in Table 1, adenine nucleotide binding may change by 8-fold for AMP-PNP, 30-fold for ADP, or >300-fold for AMP where the last nucleotide has no significant interaction with the basal-state enzyme (Figure 2). Furthermore, K_i for the phenylalanyl peptide substrate-analogue F-IRS939 was 1−2 mM in either state and is thus not significantly changed by autophosphorylation. In the case of adenine nucleotides, these studies suggest the β-phosphate may be essential for nucleotide binding in the basal-state but appears less important in the activated state (K_i values for AMP-PNP versus AMP, Table 1). Therefore, the broad range of affinity changes for adenine nucleotides is not entirely consistent with a direct steric occlusion model for activation by relief of intrasteric inhibition; i.e., one in which the nucleotide binding site is the same in the activated and basal states and the activation loop only acts as if it were a competitive inhibitor in the basal state. To the contrary, these features suggest that nucleotides are not bound in structurally equivalent conformations in the basal and activated states. For the peptide binding site, a single interpretation of binding affinities is equally elusive. In the case of F-IRS939, weak binding in the basal state may be from intrasteric inhibition, but weak binding in the activated state may result from lack of a hydrogen bonding interaction between the (absent) phenolic hydroxyl of the P0 residue and D1132 (*27*). These factors cannot be parsed from a steady-state kinetic analysis, and therefore peptide inhibition constants by themselves failed to provide useful insights into relief of intrasteric inhibition at the peptide binding site.

Changes in the Rate-Limiting Step and Changes in Substrate Binding. Rate constants determined from viscometric analysis suggest the effects of activation by autophosphorylation are restricted to steps leading up to and including the transition state complex. Product release steps may not be altered significantly following activation by autophosphorylation, assuming the lower limit for $k_{4'}$ given in Table 2 is a good approximation for product release rate in the basal-state enzyme. In the basal-state kinase, the chemistry is rate-limiting ($k_3 \ll k_{4'}$ and $\{k_{cat}\}^{\eta} = 0$), but in the activated-state kinase chemistry and product release are each partially rate-limiting (k_3 and $k_{4'}$ are of similar magnitudes and $\{k_{cat}\}^{\eta} = 0.8$). The change in k_3 produces the change in the rate-limiting step between the basal-state and activated-state kinases, and underlies the free-energy differences for binding and chemical steps in the reaction catalyzed by the activated versus the basal-state kinase (Table 3). The major effect of autophosphorylation is a 36-fold change in the chemical step's rate constant k_3 in contrast to the 7-fold change in turnover number k_{cat} determined from steady-state kinetics alone. This change was obscured within k_{cat} by the relative magnitude of the net rate constant for product release $k_{4'}$ (Table 2 and eq 7). The folds-change in *dissociation* constants for substrates are smaller than suggested by the respective Michaelis constants because the large change in k_3 is hidden within the expression $K_M = K_d k_{4'}/(k_3 + k_{4'})$. Thus the free energies of binding for each substrate are only about 1 kcal/mol more favorable following activation.[4]

Table 3: Relative Changes in Kinetic Parameters and the Associated Free Energies[a]

parameter	fold chg	$\Delta\Delta G_0$ (kcal/mol)	parameter	fold chg	$\Delta\Delta G_0$ (kcal/mol)
k_3	36	−2.1	k_{cat}	7	−1.1
$K_{d,ATP}$	5	−1.0	$K_{M,ATP}$	25	−1.9
$K_{d,Y-IRS939}$	8	−1.2	$K_{M,Y-IRS939}$	40	−2.2
$k_3/K_{d,ATP}$	180	−3.1	$k_{cat}/K_{M,ATP}$	175	−3.0
$k_3/K_{d,Y-IRS939}$	290	−3.3	$k_{cat}/K_{M,Y-IRS939}$	280	−3.3

[a] The changes in free energy were calculated from the Gibbs free energy relationship, $\Delta\Delta G_0 = -RT\ln$(fold-change) at 298 °K.

The enhanced catalytic efficiency reported by second-order rate constants k_3/K_d or k_{cat}/K_M is about 3 kcal/mol more favorable for each substrate after activation because of the 36-fold increased rate for the chemical step of the reaction more so than the 5- or 8-fold tighter binding of that substrate. This can be seen from the free energy-reaction profile shown in Figure 4. From independent experiments (*21*), it was shown that the activated IRKD has 3.9 kcal/mol *less* intrinsic conformational free energy than the basal-state IRKD ($\Delta\Delta G_{H_20}$); this difference is indicated by the relative free energies of the enzyme prior to substrate binding (E + T + Y). The basal-state IRKD is assigned an arbitrary free energy of zero as a reference value. The ternary complex (ETY) in the activated state is 1.7 kcal/mol *less* stable than the same complex in the basal state, despite the fact that substrate binding affinity has increased 5-fold for MgATP and 8-fold for peptide substrate (Table 3). Furthermore, the difference in ternary complexes deduced from these relative free energies is consistent with different structural requirements for adenine nucleotide binding deduced from variations in K_i values, as described above. The free energy barrier to reach the transition state in the forward direction ($\Delta G^{\ddagger}$) is 17.6 kcal/mol for the basal-state enzyme and 15.4 kcal/mol for the activated enzyme, a net difference of 2.2 kcal/mol in favor of the activated kinase. However, the net difference in relative free energy of the transition state complex is only 0.5 kcal/mol in favor of the activated enzyme.

To calculate relative free energies of the ternary complexes with products (EDpY), we need a value for the internal equilibrium between ternary complexes, K_{tc}, which can be determined from the overall equilibrium K_{eq} and kinetic parameters. The steps of the enzyme-catalyzed reaction, shown in Scheme 2, frames the overall equilibrium between products MgADP (D) and phosphotyrosyl peptide (pY), and the substrates MgATP (T) and tyrosyl-peptide (Y)

$$K_{eq} = \frac{[D][pY]}{[T][Y]} = K_{tc}\frac{K_{d,D}K_{d,pY}}{K_{d,T}K_{d,Y}} \qquad (13)$$

[4] It is possible to calculate the on- and off-rate constants for substrate binding, given the dissociation constants in Table 2. Thus, for peptide substrate, $k_{-2} \geq 12\ s^{-1}$ because $k_{-2} \gg k_3$ in the basal state follows from the lack of viscosity dependence for k_{cat}/K_M (Figure 3), and $k_2 \geq 6 \times 10^3\ M^{-1}\ s^{-1}$ is calculated from $k_2 = k_{-2}/K_d$. For the activated state, these parameters are estimated to be $k_2 \approx 2 \times 10^6\ M^{-1}\ s^{-1}$ and $k_{-2} = 500\ s^{-1}$, using the same approach. Because these numbers are highly dependent on other calculated parameters and therefore large errors must apply, the actual values are much less important than the qualitatively accurate observation that substrate binding equilibrates faster than the chemical step of the catalytic cycle, as described in the text.

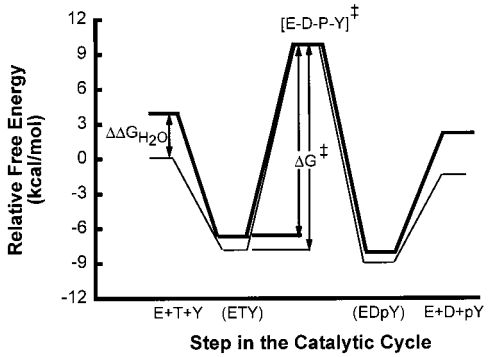

FIGURE 4: Free energy profile for peptide phosphorylation by the insulin receptor's kinase domain. The free energies for five steps in the kinase-catalyzed phosphorylation of Y-IRS939 (Y) by MgATP (T) are shown for the basal-state (thin line) and activated-state kinase (thick line). The reference state for the reaction is the basal-state kinase and its unbound substrates with an arbitrary value $\Delta G_{0,S} = 0$ kcal/mol, where the subscript S or P indicates substrate- or product-associated steps. The activated kinase is less stable by 3.9 kcal/mol ($\Delta G_0 = +3.9$ kcal/mol), determined by denaturation studies ($\Delta\Delta G_{H_2O}$ from ref *21*). Each ternary complex free energy was calculated relative to the dissociated substrates from the equation $\Delta\Delta G_{tc} = \Delta G_{0,S} - RT\ln(K_{d,T}K_{d,Y})$, and the ternary complexes relative to products from the equation $\Delta\Delta G_{tc} = \Delta G_{0,P} - RT\ln(K_{i,D}K_{i,pY})$, where R is the gas constant, T is the absolute (room) temperature (298 °K), and binding constants are found in Table 2 (K_i) and Table 3 (K_d). The value of $\Delta G_{0,P}$ is 1.4 kcal/mol lower than $\Delta G_{0,S}$ because $\Delta G_{0,P} - \Delta G_{0,S} = -RT\ln(K_{eq})$ and $K_{eq} = 10$, as described in the text. The difference in free energy between each ternary complex and the transition state was calculated from the rate constant for the chemical step (k_3 in Table 3) using Eyring's equation $k_3 = kTK^{\ddagger}/\hbar$ where k is Boltzmann's constant, $\hbar$ is Planck's constant, and $K^{\ddagger}$ is the "equilibrium" between transition state and ground-state complexes, yielding $\Delta G^{\ddagger} = -RT\ln[k_3{\cdot}\hbar/(kT)]$ relative to each ternary complex.

Scheme 2

$$\mathrm{E} \underset{k_{-1}}{\overset{k_1(T)}{\rightleftharpoons}} \mathrm{E{\cdot}T} \underset{k_{-2}}{\overset{k_2(Y)}{\rightleftharpoons}} \mathrm{E{\cdot}T{\cdot}Y} \underset{k_{-3}}{\overset{k_3}{\rightleftharpoons}} \mathrm{E{\cdot}D{\cdot}pY} \underset{k_{-4}(pY)}{\overset{k_4}{\rightleftharpoons}} \mathrm{E{\cdot}D} \underset{k_{-5}(D)}{\overset{k_5}{\rightleftharpoons}} \mathrm{E}$$

The equilibrium, by definition using the middle ratio, is independent of the presence or absence of enzyme and therefore independent of whether the enzyme is in its basal or activated state. On the basis of parameters determined from other protein tyrosine kinases, an average value of $K_{eq} = 10$ for tyrosyl-peptide phosphorylation is derived from the literature.[5] Product inhibition constants K_i can be used in place of product dissociation constants K_d as described by Cleland (*55*). Using K_i values from Table 1 and K_d values from Table 2, we calculate similar values for K_{tc} in the activated versus basal kinase-catalyzed reactions (9.8 versus 6.5, respectively). Thus the product ternary complex is 1.4 to 1.1 kcal/mol more stable than the corresponding substrate ternary complex, and products are favored over substrates by 1.4 kcal/mol. These calculated values for K_{tc} are consistent with the assumption that $k_3 > k_{-3}$ made in deriving expressions for viscosity dependence (eqs 7−9 and 10−12). For comparison, the phosphorylation of seryl-peptide substrates by MgATP catalyzed by PKA (*56*) and by calcium/calmodulin-dependent protein kinase II (*57*) yield $K_{eq} = 2000$ and $K_{eq} = 3500$, respectively; $K_{tc} = 100$ for PKA (*58*).

This analysis shows that the largest free energy difference between the basal and activated enzymes is inherent in the protein itself after autophosphorylation. As we had suggested previously, this *loss* of conformational free energy in the phosphorylated protein is quantitatively sufficient to account for the 200-fold increased catalytic efficiency determined from the fold-change in k_{cat}/K_M (*21*). The free energy changes across the reaction apply to the system that encompasses the protein plus the reacting species. In a broader thermodynamic sense, it is true that interactions between enzyme and the transition state ligands *together* with side chain and backbone interactions throughout the protein sum to approximately the same value in both activated and basal states. However, the most economical explanation to account for the small difference in relative free energies of the transition state complexes is to expect only small differences in active site geometries and bonds during the chemical step of the reaction; it is the same reaction catalyzed by the enzyme in its basal and activated states. Thus, whether the activation loop is phosphorylated may have little direct impact on the transition state. Instead, the higher barrier to reach the transition state should result from a residual unfavorable interaction remaining in the basal state ternary complex. The fact that net conformational free energy was lost upon autophosphorylation indicates that greater mobility can exist in the activated enzyme (*21*). This greater mobility should be as important for the chemical step of the reaction as steric freedom in the active site is for tighter substrate binding. In structural terms, it is generally accepted that lobe movement must occur during the catalytic cycle (*22*), and Hubbard has shown the activation loop is an impediment to such movement in the basal state protein without substrates bound (*18*). Taken together with the analysis presented here, we suggest that an impediment to lobe rotation persists when substrates are bound to the basal-state enzyme, and this is responsible for the slower rate of the chemical step of phosphoryl transfer. These structural features should be sufficient to explain the differences in free energy-reaction profiles in Figure 4. Therefore, the change in conformational free energy inherent in the protein after autophosphorylation (*21*) is equally distributed between formation of the substrate ternary complex and formation of the transition state complex.

The novel finding that conformational free energy has an equal impact on substrate binding and the chemical step of this kinase's catalytic cycle may be a special feature of receptor tyrosine kinases with adjacent activation loop tyrosines, or it may be unique to the insulin receptor subfamily. In studies of PKA, it was concluded that energetically similar ternary complexes were followed by energetically different transition state complexes, thus leading to a slower chemical step in the absence of activation loop phosphorylation at T197 (*59*). Furthermore, mutagenesis and kinetic studies on the protein tyrosine kinase v-fps showed essentially the same effect of activation loop phosphorylation at Y1073 as determined for PKA, suggesting the major role

[5] Overall equilibra for tyrosyl-peptide phosphorylation from MgATP have been determined from Haldane relationships for several protein tyrosine kinases: cSrc ($K_{eq} = 20$; ref *51*), C-terminal Src kinase ($K_{eq} = 21$; ref *52*), kinase domain of the vascular endothelial growth factor receptor ($K_{eq} = 10$; ref *53*), and the epidermal growth factor receptor ($K_{eq} = 1.6$; ref *54*). A value of $K_{eq} = 1.6$ was calculated for the unphosphorylated vascular endothelial growth factor receptor kinase, which should in principle have been 17, i.e., the same as for the activated enzyme because the enzyme is not expected to perturb the equilibrium. Either a different Haldane relationship for this mechanism (*55*) should have been applied, or the measurements had an inherent but subtle error.

of activation loop phosphorylation was to increase the rate of the chemical step in phosphoryl transfer with little impact on active site accessibility (*43*). Indeed, if there is one universal function of activation loop phosphorylation it would appear to be an impact on the chemical step's rate constant, based on a comparison among three protein tyrosine kinases that have zero, one, or two activation loop phosphotyrosines: $k_3 = 1.2\ s^{-1}$ for C-terminal Src kinase which is always at zero loop phosphotyrosine (calculated from Figure 3 of ref. *52*), $k_3 = 0.2-3.0\ s^{-1}$ for v-fps with zero loop phosphotyrosine versus $k_3 \approx 40\ s^{-1}$ with one loop phosphotyrosine (*36*, *43*), and $k_3 = 1.2\ s^{-1}$ versus $42\ s^{-1}$ for the IRKD for zero versus two loop phosphotyrosines (Table 2). While we have followed these other studies in using steady-state kinetics and viscometric analysis, we have also brought forward denaturation data to establish conformational free energies of the basal- and activated-state IRKD in solution. This combined approach has revealed a unique mechanistic feature of the reaction catalyzed by the insulin receptor's kinase domain and may prove fundamentally useful to further our understanding of the relationships between crystal structures and catalytic mechanisms.

ACKNOWLEDGMENT

The authors thank Joseph Adams, Philip Cole (IRS727 peptides), J. B. Alexander Ross, and Stevan Hubbard for helpful discussions. This work was supported by NIH Grant DK50074.

REFERENCES

1. Heldin, C. H. (1995) *Cell 80*, 213−223.
2. Koch, C. A., Anderson, D., Moran, M. F., Ellis, C., and Pawson, T. (1991) *Science 252*, 668−674.
3. Lane, M. D., Ronnett, G. V., Kohanski, R. A., and Simpson, T. L. (1985) *Curr. Top. Cell Regul. 27*, 279−292.
4. White, M. F., and Kahn, C. R. (1994) *J. Biol. Chem. 269*, 1−4.
5. Ebina, Y., Ellis, L., Jarnagin, K., Edery, M., Graf, L., Clauser, E., Ou, J. H., Masiarz, F., Kan, Y. W., Goldfine, I. D., et al. (1985) *Cell 40*, 747−758.
6. Villalba, M., Wente, S. R., Russell, D. S., Ahn, J. C., Reichelderfer, C. F., and Rosen, O. M. (1989) *Proc. Natl. Acad. Sci. U.S.A. 86*, 7848−7852.
7. Kohanski, R. A., and Schenker, E. (1991) *Biochemistry 30*, 2406−2414.
8. Kohanski, R. A. (1993) *Biochemistry 32*, 5766−5772.
9. Kohanski, R. A. (1993) *Biochemistry 32*, 5773−5780.
10. Cobb, M. H., Sang, B. C., Gonzalez, R., Goldsmith, E., and Ellis, L. (1989) *J. Biol. Chem. 264*, 18701−18706.
11. Tavare, J. M., Clack, B., and Ellis, L. (1991) *J. Biol. Chem. 266*, 1390−1395.
12. Flores-Riveros, J. R., Sibley, E., Kastelic, T., and Lane, M. D. (1989) *J. Biol. Chem. 264*, 21557−21572.
13. Wei, L., Hubbard, S. R., Hendrickson, W. A., and Ellis, L. (1995) *J. Biol. Chem. 270*, 8122−8130.
14. Zhang, B., Tavare, J. M., Ellis, L., and Roth, R. A. (1991) *J. Biol. Chem. 266*, 990−996.
15. Murakami, M. S., and Rosen, O. M. (1991) *J. Biol. Chem. 266*, 22653−22660.
16. Tornqvist, H. E., and Avruch, J. (1988) *J. Biol. Chem. 263*, 4593−4601.
17. Hubbard, S. R., Wei, L., Ellis, L., and Hendrickson, W. A. (1994) *Nature 372*, 746−754.
18. Hubbard, S. R. (1997) *EMBO J. 16*, 5572−5581.
19. Kobe, B., Heierhorst, J., and Kemp, B. E. (1997) *Adv. Second Messenger Phosphoprotein Res. 31*, 29−40.
20. Frankel, M., Bishop, S. M., Ablooglu, A. J., Han, Y. P., and Kohanski, R. A. (1999) *Protein Sci. 8*, 2158−2165.
21. Bishop, S. M., Ross, J. B., and Kohanski, R. A. (1999) *Biochemistry 38*, 3079−3089.
22. Williams, J. C., Wierenga, R. K., and Saraste, M. (1998) *Trends Biochem Sci. 23*, 179−184.
23. Hubbard, S. R., Mohammadi, M., and Schlessinger, J. (1998) *J. Biol. Chem. 273*, 11987−11990.
24. Sun, X. J., Rothenberg, P., Kahn, C. R., Backer, J. M., Araki, E., Wilden, P. A., Cahill, D. A., Goldstein, B. J., and White, M. F. (1991) *Nature 352*, 73−77.
25. Myers, M. G., Jr., Zhang, Y., Aldaz, G. A., Grammer, T., Glasheen, E. M., Yenush, L., Wang, L. M., Sun, X. J., Blenis, J., Pierce, J. H., and White, M. F. (1996) *Mol. Cell. Biol. 16*, 4147−4155.
26. Cann, A. D., Wolf, I., and Kohanski, R. A. (1997) *Anal. Biochem. 247*, 327−332.
27. Ablooglu, A. J., Till, J. H., Kim, K., Parang, K., Cole, P. A., Hubbard, S. R., and Kohanski, R. A. (2000) *J. Biol. Chem. 275*, 30394−30398.
28. Whittaker, J., Okamoto, A. K., Thys, R., Bell, G. I., Steiner, D. F., and Hofmann, C. A. (1987) *Proc. Natl. Acad. Sci. U.S.A. 84*, 5237−5241.
29. Cann, A. D., and Kohanski, R. A. (1997) *Biochemistry 36*, 7681−7689.
30. Cann, A. D., Bishop, S. M., Ablooglu, A. J., and Kohanski, R. A. (1998) *Biochemistry 37*, 11289−11300.
31. Dixon, M., and Webb, E. C. (1979) *Enzymes*, 3rd ed., Academic Press, New York.
32. Rudolph, F. B., and Fromm, H. J. (1979) *Methods Enzymol. 63*, 138−159.
33. Cleland, W. W. (1979) *Methods Enzymol. 63*, 103−138.
34. Walker, D. H., Kuppuswamy, D., Visvanathan, A., and Pike, L. J. (1987) *Biochemistry 26*, 1428−1433.
35. Birdsall, B., King, R. W., Wheeler, M. R., Lewis, C. A., Jr., Goode, S. R., Dulap, R. B., and Roberts, G. C. (1983) *Anal. Biochem. 27*, 353−361.
36. Wang, C., Lee, T. R., Lawrence, D. S., and Adams, J. A. (1996) *Biochemistry 35*, 1533−1539.
37. Blacklow, S. C., Raines, R. T., Lim, W. A., Zamore, P. D., and Knowles, J. R. (1988) *Biochemistry 27*, 1158−1167.
38. Cole, P. A., Burn, P., Takacs, B., and Walsh, C. T. (1994) *J. Biol. Chem. 269*, 30880−30887.
39. Chlebowski, J. F., and Coleman, J. E. (1974) *J. Biol. Chem. 249*, 7192−7202.
40. Grace, M. R., Walsh, C. T., and Cole, P. A. (1997) *Biochemistry 36*, 1874−1881.
41. Freifelder, D. (1982) *Physical Biochemistry: Applications to Biochemistry and Molecular Biology*, 2nd ed., W. H. Freeman, San Francisco.
42. Adams, J. A., and Taylor, S. S. (1992) *Biochemistry 31*, 8516−8522.
43. Saylor, P., Hanna, E., and Adams, J. A. (1998) *Biochemistry 37*, 17875−17881.
44. Pocker, Y., and Janjic, N. (1987) *Biochemistry 26*, 2597−2606.
45. Skamnaki, V. T., Owen, D. J., Noble, M. E., Lowe, E. D., Lowe, G., Oikonomakos, N. G., and Johnson, L. N. (1999) *Biochemistry 38*, 14718−14730.
46. Prowse, C. N., Hagopian, J. C., Cobb, M. H., Ahn, N. G., and Lew, J. (2000) *Biochemistry 39*, 6258−6266.
47. Snider, M. J., Gaunitz, S., Ridgway, C., Short, S. A., and Wolfenden, R. (2000) *Biochemistry 39*, 9746−9753.
48. Shoelson, S. E., White, M. F., and Kahn, C. R. (1989) *J. Biol. Chem. 264*, 7831−7836.
49. Kasuga, M., Fujita-Yamaguchi, Y., Blithe, D. L., White, M. F., and Kahn, C. R. (1983) *J. Biol. Chem. 258*, 10973−10980.
50. Kohanski, R. A. (1989) *J. Biol. Chem. 264*, 20984−20991.
51. Boerner, R. J., Barker, S. C., and Knight, W. B. (1995) *Biochemistry 34*, 16419−16423.

52. Cole, P. A., Grace, M. R., Phillips, R. S., Burn, P., and Walsh, C. T. (1995) *J. Biol. Chem. 270*, 22105−22108.
53. McTigue, M. A., Wickersham, J. A., Pinko, C., Showalter, R. E., Parast, C. V., Tempczyk-Russell, A., Gehring, M. R., Mroczkowski, B., Kan, C. C., Villafranca, J. E., and Appelt, K. (1999) *Struct. Fold Des. 7*, 319−330.
54. Hubler, L., Gill, G. N., and Bertics, P. J. (1989) *J. Biol. Chem. 264*, 1558−1564.
55. Cleland, W. W. (1963) *Biochim. Biophys. Acta 67*, 104−137.
56. Qamar, R., Yoon, M. Y., and Cook, P. F. (1992) *Biochemistry 31*, 9986−9992.
57. Kwiatkowski, A. P., Huang, C. Y., and King, M. M. (1990) *Biochemistry 29*, 153−159.
58. Adams, J. A., and Taylor, S. S. (1993) *Protein Sci. 2*, 2177−2186.
59. Adams, J. A., McGlone, M. L., Gibson, R., and Taylor, S. S. (1995) *Biochemistry 34*, 2447−2454.

BI002292M